

Antiferromagnetic droplet soliton driven by spin current

Roman V. Ovcharov,¹ Mohammad Hamdi,^{2,3} Boris A. Ivanov,^{4,5} Johan Åkerman,^{1,6,7} and Roman S. Khymyn¹

¹*Department of Physics, University of Gothenburg, Gothenburg 41296, Sweden*

²*Ecole Polytechnique Federale de Lausanne (EPFL), Institute of Materials, Laboratory of Nanoscale Magnetic Materials and Magnonics, CH-1015 Lausanne, Switzerland*

³*Department of Electrical and Computer Engineering, Northwestern University, Evanston, IL 60208, USA*

⁴*Institute of Magnetism of NASU and MESU, Kyiv 03142, Ukraine*

⁵*Radboud University, Institute for Molecules and Materials, Nijmegen 6525 AJ, Netherlands*

⁶*Center for Science and Innovation in Spintronics, Tohoku University, Sendai 980-8577, Japan*

⁷*Research Institute of Electrical Communication, Tohoku University, Sendai 980-8577, Japan*

(Dated: 1 December 2023)

We demonstrate that a spin current flowing through a nano-contact into a uniaxial antiferromagnet with first- and second-order anisotropy can excite a self-localized dynamic magnetic soliton, known as a spin-wave droplet in ferromagnets. The droplet nucleates at a certain threshold current with the frequency of the Néel vector precession laying below the antiferromagnetic resonance. The frequency exhibits nonlinear behavior with the increasing of applied current. At the high value of applied torque, the soliton mode transforms, and the oscillator emits spin waves propagating in the antiferromagnetic layer.

Antiferromagnetic materials (AFMs) have unique properties advantageous for future spintronic applications, including the absence of stray fields, intrinsic high-frequency dynamics, high spin wave velocities, and abundance in nature^{1,2}. Utilizing their terahertz (THz) spin dynamics due to strong exchange interaction can bring about solid-state THz nano-devices and, hence, close the THz gap^{3,4}. One of the most promising candidates of such devices is the AFM-based spin-Hall and spin-transfer torque nano-oscillators (SH/ST-NOs), which can operate as THz sources and detectors^{5–17}. Furthermore, these devices offer great potential for on-chip THz neuromorphic applications^{16–20}. Several attempts have been made to understand current-driven spin dynamics in single SH/ST-NOs^{5–17}, which can further be coupled by propagating THz Slonczewski spin waves²¹, similar to ferromagnetic counterparts^{22–26}.

Employing *localized* spin dynamics is of crucial importance for the operation of spintronics devices^{27,28}. Contrary to ferromagnets (FMs), where a combination of demagnetization, crystal anisotropy, and external field can form the localizing potential for magnons, the localization of spin dynamics in AFMs is challenging. It can be achieved by exciting self-localized AFM spin textures such as domain walls, Bloch lines, and skyrmions^{28–30}, however pure dynamical localized excitations can substantially enrich the scopes of AFM devices. Such dynamical states in the form of AFM solitons were predicted theoretically a long time ago^{31–33} in the case of zero damping. However, their practical realization was unresolved due to the lack of any excitation method. In contrast, FM dynamic solitons, such as droplets, are experimentally demonstrated in SH/ST-NOs^{34–39}.

In this Letter, we study the excitation of dissipative AFM droplet solitons in a nanocontact (NC)-based SH/ST-NO. We use micromagnetic simulations to investigate the stability and properties of the excited AFM droplets as a function of applied current, magnetic anisotropies, and NC radius. In particular, we compare

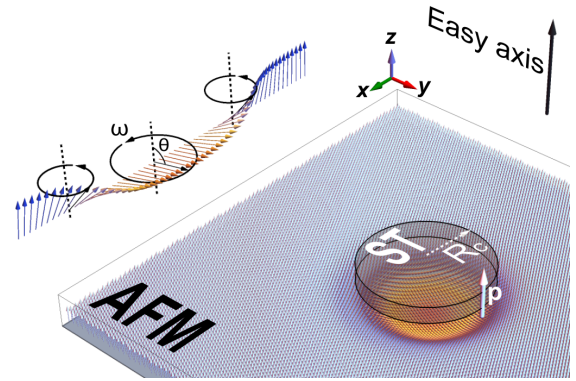


FIG. 1. Schematic illustration of an AFM ST oscillator. The nanocontact, which acts as a spin current source, is placed on top of a thin AFM layer with uniaxial anisotropy. The black arrow shows the easy-axis orientation, and the white arrow indicates the direction of the spin current polarization. In the upper left corner, a sketch of the Néel vector precession shows the spin structure across the excited droplet.

droplet structures for different NC radii and evaluate their influence on the output signal. Our choice of material is Ru- and Rh-doped hematite (α - Fe_2O_3), which has been identified as a promising candidate for potential experimental realization⁴⁰.

Analytical model. We consider a scheme that is widely used for the excitations of the droplets in ferromagnets and is shown in Fig. 1. It consists of an AFM thin film and adjunct NC that is a source of spin current, providing spin-transfer or spin-orbit torque onto the AFM magnetic sublattices. The AFM has uniaxial anisotropy, and spin current is polarized along the easy axis. In ferromagnets strong enough out-of-plane anisotropy, overcoming the demagnetizing field, creates attractive coupling between magnons, which is necessary for a self-formation of droplet-like solitons^{34,35,41}. Contrary to ferromagnets, simple quadratic anisotropy (in the form $-K_1 M_z^2$)

does not provide nonlinear coupling between magnons in AFMs. It was proposed in Refs. 31 and 32 to employ higher-order terms in the anisotropy energy density as

$$w_a = -K_1 \cos^2 \theta - K_2 \cos^4 \theta, \quad K_1, K_2 > 0 \quad (1)$$

to stabilize droplets, where θ is the angle between easy-axis and Néel vector. This anisotropy together with the exchange field H_{ex} defines two characteristic frequencies of the AFM: for the small amplitude precession ($\theta \simeq 0$): $\omega_{AFMR} = \gamma \sqrt{H_{ex}(K_1 + 2K_2)}/M_s$ and the maximum one ($\theta \simeq \pi/2$): $\omega_{SF} = \gamma \sqrt{H_{ex}K_1}/M_s$.

Eq. 1 is reported to describe magnetic anisotropies in hematite⁴². These anisotropy terms can be tuned by doping elements⁴³ in hematite. For example, it is shown that Ru and Rh (Al and Ga) doping increase (decrease) both K_1 and K_2 ⁴³. The exchange field can also be reduced by any doping in hematite^{44,45}. These properties make hematite an ideal candidate for realizing AFM droplets in experiments.

The conservative dynamics of the AFM droplet can be described in terms of the angular variables for the Néel vector θ and ϕ , where ϕ is the angle in the hard plane. The soliton solution is $\theta = \theta(r)$ and $\phi = \omega t$, where $\theta(r)$ is governed by the equation:

$$2r_0^2 \left(\frac{d^2\theta}{dr^2} + \frac{1}{r} \frac{d\theta}{dr} \right) + \sin 2\theta \left(\frac{\omega^2 - \omega_c^2}{\omega_{AFMR}^2 - \omega_c^2} - \cos 2\theta \right) = 0.$$

This equation together with the boundary conditions $\theta'(0) = 0$, $\theta(\infty) = 0$, defines the profile of the soliton at a given frequency ω (in the range $\omega_c < \omega < \omega_{AFMR}$) with $\theta(0) = \theta_0$ at the center of the droplet. Here $\omega_c = \sqrt{(\omega_{AFMR}^2 + \omega_{SF}^2)}/2$ is the minimum frequency and $r_0 = c/\sqrt{\omega_{AFMR}^2 - \omega_c^2}$ is a characteristic size of a soliton, c is the maximum speed of magnons defined by the exchange interaction³¹. As we will see below, r_0 is an important parameter of the AFM material since it defines the required geometry of the NC for the droplet excitation. The frequency of precession ω is the single variable of the droplet, and its profile can be defined completely at a given ω and analyzed numerically.

The excitation of a *dissipative* droplet by spin current passing through the NC with the radius R_c , Fig. 1, requires to account the energy balance between the gain and dissipation across the soliton profile. In the stationary regime of a droplet precession, this condition can be expressed as:

$$\Gamma_{tot} = \sigma j \int_0^{R_c} \dot{\phi} \sin^2 \theta r dr - \alpha \int_0^\infty \dot{\phi}^2 \sin^2 \theta r dr = 0, \quad (2)$$

where α is a Gilbert damping constant, j is an electrical current density and σ describes ST efficiency. The condition of the Eq. (2) selects the particular frequency and, hence, the profile of a droplet.

The above approach is highlighted in Fig. 2, where Γ_{tot} and droplet profiles are shown at different currents. At

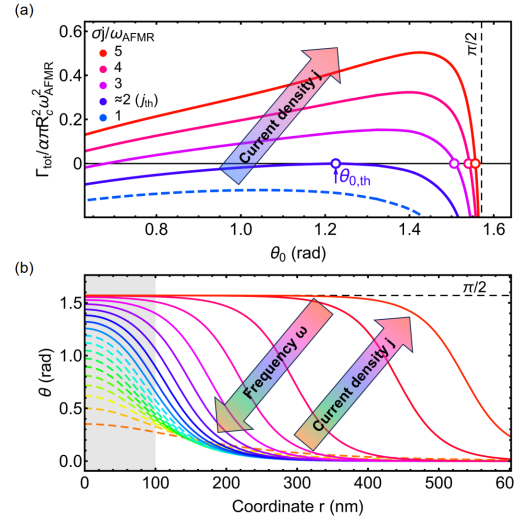


FIG. 2. a) Dependence Γ_{tot} on θ_0 for different values of the applied current. The condition $\Gamma_{tot} = 0$ selects the b) profile of the soliton. Profiles with $\theta_0 < \theta_{0,th}$ are shown by dashed lines. Here $\omega_{AFMR}/2\pi = 213$ GHz, $\omega_c/2\pi = 192$ GHz, $r_0 = 40$ nm and $R_c = 100$ nm. The direction of the current increase is highlighted by the arrow.

the low value of applied current $\Gamma_{tot} < 0$ for all possible θ_0 and the droplet is absent. However at a certain threshold j_{th} a solution $\Gamma_{tot} = 0$ appears with a finite value of $\theta_0 = \theta_{0,th}$, which in turn corresponds to a droplet frequency $\omega_{th} < \omega_{AFMR}$. At higher currents, the condition $\Gamma_{tot} = 0$ has two solutions; however, the left one is unstable against an increase in droplet amplitude. While a soliton expands with a current, its frequency gradually decreases towards the limit value ω_c .

Micromagnetic simulations. To investigate the dynamics of an AFM droplet, we carried out micro-magnetic simulations using MuMax3 solver⁴⁶ for a system illustrated in Fig. 1. The structure is composed of an AFM film measuring 516×516 nm² with a thickness of 7 nm. At the center of the device, a circular NC having a radius of R_c is placed, supplying a spin current polarized along the easy axis of the AFM. The AFM material properties are set to correspond to α -Fe₂O₃^{40,42,47-51}, with sublattice saturation magnetization $M_s = 860$ kA/m, exchange stiffness $A_{ex} = 7.7$ pJ/m, exchange field $H_{ex} = 1800$ T. The intrinsic damping of hematite is rather low (see, e.g., Ref. 50 with reported $\alpha = 1.1 \times 10^{-5}$), but to account for the damping enhancement due to the spin pumping, we set it to $\alpha = 10^{-3}$. Similar to the static spin-flop with magnetic anisotropy given by Eq. 1, the excitation induced by the spin current exhibits hysteresis behavior. Consequently, our simulations commence at a higher current, followed by a gradual decrease to the operational value. Hence, the *threshold* current refers to the minimal operational current that maintains excitations. The primary parameters include the excitation frequency ω under the NC center and the amplitude defined by the deflection angle θ_0 at the same point. To ensure that the

excitation corresponds to the droplet mode, we check for the condition for frequency to be lower than AFM resonance $\omega < \omega_{\text{AFMR}}$, where propagating magnons are absent in bulk AFM.

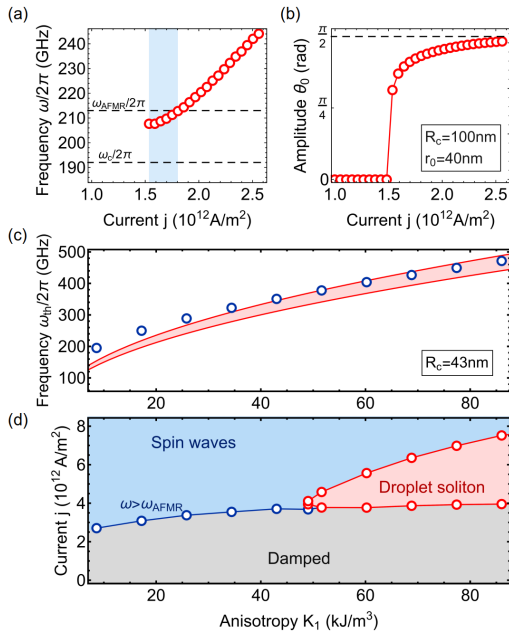


FIG. 3. The dependences of (a) the precession frequency $\omega/2\pi$ and (b) the deflection angle θ_0 on the applied current density for the NC with $R_c = 100$ nm and characteristic length $r_0 = 40$ nm ($K_1 = 16.3$ kJ/m 3). The dependences on the anisotropy constants of (c) the excitation frequency at the threshold and (d) the “phase diagram” of the excitation type as a function of the applied current density. The red-filled region in (c) shows the theoretical limits of the droplet frequency in the non-dissipative limit, indicated by the horizontal dashed lines in (a). The blue bar in (a) highlights the range of currents at which the droplet is observed.

First, we analyzed the case of anisotropy values corresponding to undoped hematite given by $K_1 = 16.3$ kJ/m 3 and $K_2 = 4.9$ kJ/m 3 , which gives the characteristic length $r_0 = 40$ nm for the maximum speed of $c = 23$ km/s. The results of excitation by NC with $R_c = 100$ nm are shown in Fig. 3 (a, b). Notably, a gap between the frequency of the excitation and AFMR appears at the threshold $j_{\text{th}} = 1.54 \times 10^{12}$ A/m 2 , similar to what is observed for the droplets in ferromagnetic oscillators. This gap results from an amplitude threshold for the droplet excitation $\theta_0 > \theta_{0,\text{th}}$ discussed above. As the current increases to $j_{\text{sw}} = 1.8 \times 10^{12}$ A/m 2 , the area under the NC starts to emit propagating spin waves instead of the localized droplet. The frequency and applied current range within which the droplet persists is relatively narrow. Furthermore, if the NC radius is reduced to the characteristic size of r_0 , the initiation of the localized droplet ceases at any current value, yielding only propagating spin waves.

In order to excite droplets at smaller NC radii, the

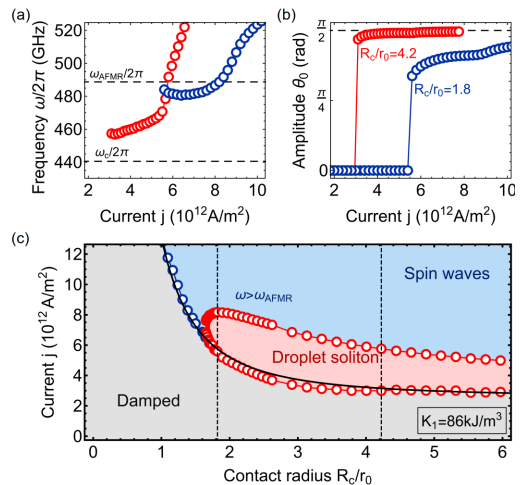


FIG. 4. The dependences of (a) the precession frequency $\omega/2\pi$ and (b) the deflection angle θ_0 on the applied current density for the NC with a radius of (red) 73 nm and (blue) 31 nm. (c) The “phase diagram” of the excitation type as a function of the NC radius and applied current density; vertical dashed lines indicate selected radii used in (a) and (b). The solid black line is calculated using Eq. (3) from Ref. 21. Characteristic length $r_0 = 17.3$ nm.

droplet’s characteristic size should be reduced. To achieve this, we investigated the impact of increasing anisotropy values K_1 and K_2 , keeping their ratio constant at $\rho = K_2/K_1 = 0.3$. Ru and Rh doping would help reduce the droplet characteristic size by increasing the anisotropies and decreasing the exchange field, hence, c . The results of simulations, with a NC radius of 43 nm, are depicted in Figure 3 (c, d). For anisotropy values up to $K_1 \approx 50$ kJ/m 3 , the excitation frequency at the threshold exceeds the AFMR, and the localization is not forming. At around $K_1 \approx 50$ kJ/m 3 the localized droplet region is emerging within a narrow range of applied current, but with the subsequent increase in anisotropy, the region of a droplet excitation extends across a broader range of both frequency and current due to the reduction in the characteristic length r_0 .

Now, we advance to analyze the dependences on NC radius R_c . For this, we set the anisotropy constants as $K_1 = 86.0$ kJ/m 3 and $K_2 = 25.8$ kJ/m 3 , thereby determining the characteristic size r_0 to equal 17.3 nm. Figure 4 shows the diagram of excitation types depending on the R_c/r_0 ratio and the applied current density. A scenario solely characterized by the excitation of propagating spin waves is observed for small NC radii, $R_c \lesssim 1.5r_0$. Pure droplets can be excited at NC radii larger than the characteristic size, yet the region is limited by transforming at j_{sw} to a novel object, where droplet excites propagating spin waves. Interestingly, the dependence of the lower threshold on the NC radius corresponds to the one of Slonczewski mode⁵², which is described in Ref. 21 (Eq.3) for the AFM case. Thus, the maintenance threshold, shown by the solid black line in Fig. 4 (c), is calcu-

lated using Eq. (3) in Ref. 21 with the substitution $\omega_A \rightarrow \omega_{\text{SF}}^2/\omega_{\text{ex}}$, while the nucleation threshold can be described using $\omega_A \rightarrow \omega_{\text{AFMR}}^2/\omega_{\text{ex}}$, $\omega_{\text{ex}} = \gamma H_{\text{ex}}$.

The profile of the droplet, as well as the frequency, also depend on the R_c/r_0 ratio, and we examine droplet features for two NC radii: $R_c = 1.8r_0$ and $R_c = 4.2r_0$. For a small NC radius, in example $R_c = 1.8r_0$, the frequency range is narrow, akin to the above observations made with smaller anisotropy, see Fig. 3. However, the broader current span allows observing a theoretical prediction that suggests a frequency lowering with increased energy influx and, consequently, increased soliton amplitude θ_0 . Contrarily, when dealing with a larger NC radius of $R_c = 4.2r_0$, the droplet exhibits a considerably broader frequency range, implying improved tunability. However, this case is characterized by an almost 90° precession angle across the current range. This characteristic reduces the output torque $\tau_{\text{out}} = \mathbf{l} \times \dot{\mathbf{l}}$, as the ac component of spin pumping is maximized at $\theta = 45^\circ$ and diminishes to zero during the proliferation phase^{5,21} with 90° precession angle. Nevertheless, the total signal could be non-zero since the entire droplet structure under the NC should be considered.

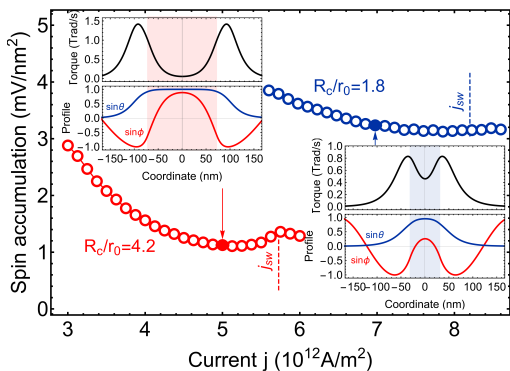


FIG. 5. Spin accumulation density, integrated over the NC region, as a function of applied current density for NCs with a radius of (red) 73 nm and (blue) 31 nm. The insets show the cross-section of the output torque distribution and the droplet profile.

For a detailed analysis of the output signals corresponding to chosen NC radii, we computed the dependence of the average spin accumulation on the applied current densities, see Fig. 5. The total spin accumulation V is the sum of the output torques generated by the precession of the Néel vectors within the NC region S , $V = (\hbar/e) \sum_S \tau_{\text{out}}$. We further determined the amplitude of the alternating component using a Fourier transform and normalized it relative to the NC areas to facilitate efficiency comparison. Hence, for a small NC radius $R_c = 1.8r_0$, the absence of planar rotation regions within the droplet profile leads to a higher spin accumulation density, although the NC with $R_c = 4.2r_0$ exhibits a higher total spin accumulation due to its larger interfacial area.

Note that contrary to the idealized model of droplet

in the AFM without dissipation, where in-plane angle ϕ is constant in space, our simulations suggest that in the dissipative soliton ϕ depends strongly on the radial coordinate r . This dependence can be described as the presence of highly nonlinear spin waves (SWs) with a frequency equal to precession frequency ω , confined within the central region of the soliton and propagating from the center of the droplet toward its edge. A qualitative explanation is, in this central area $\theta \simeq \pi/2$ and it can be treated as a local region of a spin-flop state, for which the magnon spectrum has a gapless branch. Thus, for $\omega < \omega_{\text{AFMR}}$ these SWs are localized inside the soliton, and they can propagate outside it only at $\omega > \omega_{\text{AFMR}}$. The wavevector of the SW increases with applied current, which gives rise to the frequency of the droplet (see Fig. 4). These SWs can also apply pressure to the transitional areas of the droplet, pushing them beyond the NC region⁵³ and reducing the ac output.

In conclusion, we demonstrate, both theoretically and through micromagnetic simulations, that AFM dissipative droplet soliton can be excited by applying a spin current through a NC in an extended AFM film featuring first- and second-order uniaxial anisotropy. To stabilize the AFM droplets, the NC radius must be larger than the characteristic size of the soliton. In this case, for a given anisotropy, the droplet mode is stable above a threshold current and below a switching current, at which point the excited AFM droplet transforms and starts to emit propagating waves. Thus, contrary to ferromagnets, the AFM droplet can be used as an effective emitter of high-frequency magnons propagating with high velocity, which is hard to implement by other methods⁵⁴. We show the presence of optimal values of the NC radius for maximizing output spin accumulation density and frequency tunability. We also observe the excitation of nonlinear spin waves inside the droplet, which differs from theoretical predictions under non-dissipative conditions. Based on our results, we suggest Ru and Rh-doped hematite ($\alpha\text{-Fe}_2\text{O}_3$) as a perfect material ground for the experimental realization of AFM droplet mode.

ACKNOWLEDGMENTS

This project is partly funded by the European Research Council (ERC) under the European Union's Horizon 2020 research and innovation programme (Grant TOPSPIN No 835068) and the Swedish Research Council Framework Grant Dnr. 2016-05980. M.H. thanks Swiss National Science Foundation (SNSF) for financial support via Grant No. 177550.

AUTHOR DECLARATIONS

Conflict of Interest

The authors have no conflicts to disclose.

DATA AVAILABILITY

The code and output data that support the findings of this study are available from the corresponding author upon reasonable request.

- ¹S. Zhang and Y. Tserkovnyak, “Antiferromagnet-Based Neuromorphics Using Dynamics of Topological Charges,” *Phys. Rev. Lett.* **125**, 207202 (2020).
- ²J. W. Austefjord, V. Brehm, S. Lepadatu, and A. Qaiumzadeh, “Non-volatile leaky integrate-and-fire neurons with domain walls in antiferromagnetic insulators,” *arXiv*, 2211.16845 (2022), [arXiv:2211.16845](#).
- ³C. Sirtori, “Bridge for the terahertz gap,” *Nature* **417**, 132–133 (2002).
- ⁴I. S. Osborne, “Filling the THz Gap,” *Science* (80-.). **320**, 1262b–1262b (2008).
- ⁵R. Cheng, D. Xiao, and A. Brataas, “Terahertz Antiferromagnetic Spin Hall Nano-Oscillator,” *Phys. Rev. Lett.* **116**, 207603 (2016).
- ⁶R. Khymyn, I. Lisenkov, V. Tiberkevich, B. A. Ivanov, and A. Slavin, “Antiferromagnetic THz-frequency Josephson-like Oscillator Driven by Spin Current,” *Sci. Rep.* **7**, 43705 (2017).
- ⁷O. R. Sulymenko, O. V. Prokopenko, V. S. Tiberkevich, A. N. Slavin, B. A. Ivanov, and R. S. Khymyn, “Terahertz-Frequency Spin Hall Auto-oscillator Based on a Canted Antiferromagnet,” *Phys. Rev. Appl.* **8**, 064007 (2017).
- ⁸Ø. Johansen and A. Brataas, “Spin pumping and inverse spin Hall voltages from dynamical antiferromagnets,” *Phys. Rev. B* **95**, 220408 (2017).
- ⁹R. Khymyn, V. Tiberkevich, and A. Slavin, “Antiferromagnetic spin current rectifier,” *AIP Adv.* **7**, 055931 (2017).
- ¹⁰O. Gomonay, T. Jungwirth, and J. Sinova, “Narrow-band tunable terahertz detector in antiferromagnets via staggered-field and antidamping torques,” *Phys. Rev. B* **98**, 104430 (2018).
- ¹¹V. Puliafito, R. Khymyn, M. Carpentieri, B. Azzerboni, V. Tiberkevich, A. Slavin, and G. Finocchio, “Micromagnetic modeling of terahertz oscillations in an antiferromagnetic material driven by the spin Hall effect,” *Phys. Rev. B* **99**, 024405 (2019).
- ¹²D.-K. Lee, B.-G. Park, and K.-J. Lee, “Antiferromagnetic Oscillators Driven by Spin Currents with Arbitrary Spin Polarization Directions,” *Phys. Rev. Appl.* **11**, 054048 (2019).
- ¹³I. Lisenkov, R. Khymyn, J. Åkerman, N. X. Sun, and B. A. Ivanov, “Subterahertz ferrimagnetic spin-transfer torque oscillator,” *Phys. Rev. B* **100**, 100409 (2019).
- ¹⁴R. E. Troncoso, K. Rode, P. Stamenov, J. M. D. Coey, and A. Brataas, “Antiferromagnetic single-layer spin-orbit torque oscillators,” *Phys. Rev. B* **99**, 054433 (2019).
- ¹⁵A. Parthasarathy, E. Cogulu, A. D. Kent, and S. Rakheja, “Precessional spin-torque dynamics in biaxial antiferromagnets,” *Phys. Rev. B* **103**, 024450 (2021).
- ¹⁶O. Sulymenko, O. Prokopenko, I. Lisenkov, J. Åkerman, V. Tiberkevich, A. N. Slavin, and R. Khymyn, “Ultra-fast logic devices using artificial “neurons” based on antiferromagnetic pulse generators,” *J. Appl. Phys.* **124**, 152115 (2018).
- ¹⁷R. Khymyn, I. Lisenkov, J. Voorheis, O. Sulymenko, O. Prokopenko, V. Tiberkevich, J. Åkerman, and A. Slavin, “Ultra-fast artificial neuron: generation of picosecond-duration spikes in a current-driven antiferromagnetic auto-oscillator,” *Sci. Rep.* **8**, 15727 (2018).
- ¹⁸O. Sulymenko and O. Prokopenko, “Terahertz-Frequency Spin Hall Oscillators for Logic Operations,” in *2019 IEEE 8th Int. Conf. Adv. Optoelectron. Lasers*, Vol. 2019-Septe (IEEE, 2019) pp. 533–536.
- ¹⁹O. Sulymenko and O. Prokopenko, “Logic Circuits Based on Neuron-Like Antiferromagnetic Spin Hall Oscillators,” in *2019 IEEE 39th Int. Conf. Electron. Nanotechnol.* (IEEE, 2019) pp. 132–137.
- ²⁰J. Grollier, D. Querlioz, K. Y. Camsari, K. Everschor-Sitte, S. Fukami, and M. D. Stiles, “Neuromorphic spintronics,” *Nat. Electron.* **3**, 360–370 (2020).
- ²¹M. Hamdi and D. Grundler, “Terahertz Slonczewski propagating spin waves and large output voltage in antiferromagnetic spin-Hall nano-oscillators,” *arXiv*, 2206.07844 (2022), [arXiv:2206.07844](#).
- ²²T. Kendziorczyk, S. O. Demokritov, and T. Kuhn, “Spin-wave-mediated mutual synchronization of spin-torque nano-oscillators: A micromagnetic study of multistable phase locking,” *Phys. Rev. B* **90**, 054414 (2014).
- ²³A. Houshang, E. Iacocca, P. Dürrenfeld, S. R. Sani, J. Åkerman, and R. K. Dumas, “Spin-wave-beam driven synchronization of nanocontact spin-torque oscillators,” *Nat. Nanotechnol.* **11**, 280–286 (2016).
- ²⁴A. A. Awad, P. Dürrenfeld, A. Houshang, M. Dvornik, E. Iacocca, R. K. Dumas, and J. Åkerman, “Long-range mutual synchronization of spin Hall nano-oscillators,” *Nat. Phys.* **13**, 292–299 (2017).
- ²⁵M. Zahedinejad, A. A. Awad, S. Muralidhar, R. Khymyn, H. Fulara, H. Mazraati, M. Dvornik, and J. Åkerman, “Two-dimensional mutually synchronized spin Hall nano-oscillator arrays for neuromorphic computing,” *Nat. Nanotechnol.* **15**, 47–52 (2020).
- ²⁶M. Zahedinejad, H. Fulara, R. Khymyn, A. Houshang, M. Dvornik, S. Fukami, S. Kanai, H. Ohno, and J. Åkerman, “Memristive control of mutual spin Hall nano-oscillator synchronization for neuromorphic computing,” *Nat. Mater.* **21**, 81–87 (2022).
- ²⁷O. Gomonay, V. Baltz, A. Brataas, and Y. Tserkovnyak, “Antiferromagnetic spin textures and dynamics,” *Nat. Phys.* **14**, 213–216 (2018).
- ²⁸J. Chen, M. Xu, J. Wang, L. Sheng, H. Jia, W. Wei, H. Zhang, Y. Zhang, H. Wang, R. Yuan, M. Hamdi, S. Liu, T. Chen, J.-P. Ansermet, D. Yu, D. Grundler, and H. Yu, “Deterministic switching of antiferromagnetic spin textures by chaotic magnons,” *Res. Sq.*, rs.3.rs2839142 (2023).
- ²⁹R. Ovcharov, E. Galkina, B. Ivanov, and R. Khymyn, “Spin Hall Nano-Oscillator Based on an Antiferromagnetic Domain Wall,” *Phys. Rev. Appl.* **18**, 024047 (2022).
- ³⁰R. Ovcharov, B. Ivanov, J. Åkerman, and R. Khymyn, “Antiferromagnetic Bloch Line Driven by Spin Current as Room-Temperature Analogue of a Fluxon in a Long Josephson Junction,” *Phys. Rev. Appl.* **20**, 034060 (2023).
- ³¹A. Kosevich, B. Ivanov, and A. Kovalev, “Magnetic Solitons,” *Phys. Rep.* **194**, 117–238 (1990).
- ³²I. V. Bar'yakhtar and B. A. Ivanov, “Dynamic solitons in a uniaxial antiferromagnet,” *J. Exp. Theor. Phys.* **58**, 190 (1983).
- ³³E. G. Galkina and B. A. Ivanov, “Dynamic solitons in antiferromagnets (Review Article),” *Low Temp. Phys.* **44**, 618 (2018).
- ³⁴S. M. Mohseni, S. R. Sani, J. Persson, T. N. Anh Nguyen, S. Chung, Y. Pogoryelov, P. K. Muduli, E. Iacocca, A. Eklund, R. K. Dumas, S. Bonetti, A. Deac, M. A. Hoefer, and J. Åkerman, “Spin torque-generated magnetic droplet solitons,” *Science* (80-.). **339**, 1295–1298 (2013).
- ³⁵M. Mohseni, M. Hamdi, H. F. Yazdi, S. A. H. Banuazizi, S. Chung, S. R. Sani, J. Åkerman, and M. Mohseni, “Magnetic droplet soliton nucleation in oblique fields,” *Phys. Rev. B* **97**, 184402 (2018).
- ³⁶M. Ahlberg, S. Chung, S. Jiang, A. Frisk, M. Khademi, R. Khymyn, A. A. Awad, Q. T. Le, H. Mazraati, M. Mohseni, M. Weigand, I. Bykova, F. Groß, E. Goering, G. Schütz, J. Gräfe, and J. Åkerman, “Freezing and thawing magnetic droplet solitons,” *Nat. Commun.* **13**, 2462 (2022), [arXiv:2104.14897](#).
- ³⁷S. Chung, A. Eklund, E. Iacocca, S. M. Mohseni, S. R. Sani, L. Bookman, M. A. Hoefer, R. K. Dumas, and J. Åkerman, “Magnetic droplet nucleation boundary in orthogonal spin-torque nano-oscillators,” *Nat. Commun.* **7**, 11209 (2016).
- ³⁸B. Divinskiy, S. Urazhdin, V. E. Demidov, A. Kozhanov, A. P. Nosov, A. B. Rinkevich, and S. O. Demokritov, “Magnetic

- droplet solitons generated by pure spin currents,” *Phys. Rev. B* **96**, 224419 (2017).
- ³⁹F. Macià and A. D. Kent, “Magnetic droplet solitons,” *J. Appl. Phys.* **128**, 100901 (2020), arXiv:2006.08808.
- ⁴⁰M. Hamdi, “Broadband spectroscopy and inelastic light scattering on the canted antiferromagnet hematite for antiferromagnetic magnonics,” *PhD Thesis, EPFL* (2023), 10.5075/epfl-thesis-9642.
- ⁴¹M. A. Hofer, T. J. Silva, and M. W. Keller, “Theory for a dissipative droplet soliton excited by a spin torque nanocontact,” *Phys. Rev. B* **82**, 054432 (2010).
- ⁴²A. H. Morrish, *Canted Antiferromagnetism: Hematite* (World Scientific, 1995).
- ⁴³K. Hayashi, K. Yamada, M. Shima, Y. Ohya, T. Ono, and T. Moriyama, “Control of antiferromagnetic resonance and the Morin temperature in cation doped α -Fe₂xM_xO₃ (M = Al, Ru, Rh, and In),” *Appl. Phys. Lett.* **119**, 32408 (2021).
- ⁴⁴J. M. Coey and G. A. Sawatzky, “A study of hyperfine interactions in the system (Fe_{1-x}Rh_x)₂O₃ using the Mossbauer effect (Bonding parameters),” *J. Phys. C Solid State Phys.* **4**, 2386 (1971).
- ⁴⁵E. Sváb and E. Krén, “Neutron diffraction study of substituted hematite,” *J. Magn. Magn. Mater.* **14**, 184 (1979).
- ⁴⁶A. Vansteenkiste, J. Leliaert, M. Dvornik, M. Helsen, F. Garcia-Sanchez, and B. Van Waeyenberge, “The design and verification of MuMax3,” *AIP Adv.* **4**, 107133 (2014).
- ⁴⁷R. L. Blake, R. E. Hessevick, T. Zoltai, and L. W. Finger, “Refinement of the hematite structure,” *Am. Mineral.* **51**, 123–129 (1966).
- ⁴⁸E. A. Turov and V. G. Shavrov, “Broken symmetry and magnetoacoustic effects in ferroand antiferromagnetics,” *Sov. Phys. Uspekhi* **26**, 593–611 (1983).
- ⁴⁹E. Turov, A. Kolchanov, V. Men’shenin, I. Mirsaev, and V. Nikolaev, “Symmetry and physical properties of antiferromagnets,” Fizmatlit, Moskow (2001).
- ⁵⁰M. Hamdi, F. Posva, and D. Grundler, “Spin wave dispersion of ultra-low damping hematite (α -Fe₂O₃) at GHz frequencies,” *Phys. Rev. Mater.* **7**, 054407 (2023).
- ⁵¹H. Jani, J.-C. Lin, J. Chen, J. Harrison, F. Maccherozzi, J. Schäd, S. Prakash, C.-B. Eom, A. Ariando, T. Venkatesan, and P. G. Radaelli, “Antiferromagnetic half-skyrmions and bimerons at room temperature,” *Nature* **590**, 74–79 (2021).
- ⁵²J. C. Slonczewski, “Excitation of spin waves by an electric current,” *J. Magn. Magn. Mater.* **195**, L261–L268 (1999).
- ⁵³S. K. Kim, Y. Tserkovnyak, and O. Tchernyshyov, “Propulsion of a domain wall in an antiferromagnet by magnons,” *Phys. Rev. B* **90**, 104406 (2014).
- ⁵⁴J. R. Hortensius, D. Afanasiev, M. Matthiesen, R. Leenders, R. Citro, A. V. Kimel, R. V. Mikhaylovskiy, B. A. Ivanov, and A. D. Caviglia, “Coherent spin-wave transport in an antiferromagnet,” *Nat. Phys.* **17**, 1001–1006 (2021).